

Intracavity self-induced transparency of a multilevel absorber

M. Müller, V. P. Kalosha,* and J. Herrmann

Max Born Institut für Nichtlineare Optik und Kurzzeitspektroskopie, Rudower Chaussee 6, D-12489 Berlin, Germany

(Received 5 January 1998)

Intracavity self-induced transparency of a three-level absorber is studied in the scope of solid-state laser generation of an ultrabroadband electromagnetic pulse that drives the population of all absorber levels through complete Rabi flopping. We show that at sufficient pump rates a Ti:sapphire laser forces an intracavity GaAs single quantum-well absorber, which provides an inter-valence-band transition in the THz domain in addition to two direct optical interband transitions, into the self-induced transparency regime and acts as an all-solid-state ultrabroadband pulse emitter. In dependence on the resonator bandwidth, the intracavity pulse energy and the absorber dipole moments we obtain a multilevel self-induced transparency pulse spectrum which extends from the THz domain up to the ultraviolet. The steady-state sub-10-fs pulse consists of only a few optical cycles with the high-frequency components at its leading edge and a single to subcyclic THz component at its trailing edge. [S1050-2947(98)05108-7]

PACS number(s): 42.50.Md, 42.65.Re, 42.50.Hz, 78.47.+p

I. INTRODUCTION

Solitary waves rendering a multilevel absorber transparent have been a topic of research for many years. On one hand, the interesting concept of electromagnetically induced transparency (EIT) predicts the approximately lossless propagation of matched pulses on the pump and Stokes transition in a three-level lambda system [1,2]. These matched pulses are not shape preserving, are resonant with only one of the atomic transitions, and do not induce Rabi flopping of the atomic level population. On the other hand, the concept of self-induced transparency (SIT) for strong pulses, that relies on reversible light-matter energy exchange owing to complete Rabi flopping of the population in a two-level system [3], has been extended to multilevel systems [4], predicting the simultaneous lossless propagation of secant-shape preserving, different-wavelength pulses (simultons) in a three-level absorber. Such simultons are spectrally narrow enough to be resonant with only one of the atomic transitions and they are strong enough to induce simultaneous Rabi flopping on the corresponding transitions. Simultons as copropagating different-wavelength SIT pulses in three-level systems are double-photon pulses, each pulse is one-photon resonant with the corresponding transition and hence linearly depending on its individual pulse area. In contrast, strong-field two-photon absorption on a single transition, such as a two-level system with forbidden single-photon resonance, was shown to support Lorentzian-shaped two-photon resonant self-induced transparency pulses [5] which exhibit a quadratic pulse area dependence. An experimental verification of different-wavelength two-photon SIT pulses has been achieved in three-level atomic vapors [6]. Analytical expressions for simultons in three- and five-level systems beside the twin secant shape were obtained by Hioe and Grobe [7]. Moreover, it was proposed recently [8] to use a three-level system for coherent soliton control of copropagating

different-wavelength pulses on the pump and Stokes transition, respectively.

In the present paper we develop the theory of intracavity multilevel self-induced transparency by solid-state laser generation of an ultrashort pulse which drives the absorber transitions to transparency. The strong resonant interaction which is shorter than the dephasing of the induced polarization induces complete Rabi flopping of the population on all quantum levels and returns the absorber to its initial state, which yields a multicomponent pulse spectrum with prominent spectral components at each transition of the multilevel quantum system. We denote such multiplephoton resonant, ultrabroadband pulses as multilevel self-induced transparency (MSIT) pulses. In contrast, multiphoton parametric interaction happens at pulse durations larger than the dephasing time of the induced polarization [9], hence Rabi flopping of the population is excluded and the polarization is assumed to respond instantaneously to the electric field, which allows a power series expansion of the material response in terms of nonlinear susceptibilities. As will be shown below, intracavity solid-state laser generation of ultrabroadband MSIT pulses is independent of a specific choice of initial preparations and dipole moments of the three-level system and it substantially differs from the copropagation of narrow-band simultons [4] as well as the matched pulse propagation of EIT [1].

By use of exact Maxwell-Bloch equations for real fields and polarizations without slowly varying envelopes (SVEA) and beyond the usual employed rotating wave approximation (RWA) we describe on the same footing two very recent topics of ultrafast laser physics as the generation of super-short light pulses as short as 6.5 fs [10] and the intracavity generation of THz radiation [11] both by use of an intracavity single quantum-well GaAs absorber inside a Ti:sapphire laser. We adopt a three-level absorber model with dipole active transitions between all levels corresponding to a GaAs absorber with one conduction but two valence, heavy hole (hh) and light hole (lh), bands. By excitation of such a bulk GaAs absorber with sub-20-fs Ti:sapphire light pulses the generation of single-cycle near-infrared THz pulses [12] as

*On leave from Institute for Nuclear Problems, Belarus State University, Minsk, Belarus.

well as hh-lh quantum beats in the THz domain by direct interband transitions [13] was shown. Tunable THz emission from a single quantum-well GaAs absorber that is due to inter-valence-band transitions induced by simultaneous short pulse excitation of hh and lh excitons was reported in Ref. [14]. Inter-valence-band hh-lh transitions can be viewed as coherent charge oscillations between hh and lh states [14]. The direct observation of THz emission accompanied with ultrashort light-pulse induced coherent charge oscillations in double and single quantum-well structures [14–16] as well as Bloch oscillations in a superlattice in the Wannier-Stark regime [17] marks an important step forward in current semiconductor physics. The optically induced THz radiation in double quantum wells by coherent interwell charge oscillations due to resonant tunneling [15] as well as in single quantum wells by inter-valence-band transitions between hh and lh states [14] or intersubband transitions in the confined conduction band [16] has been described by coherent multisubband semiconductor Bloch equations in Refs. [18–20]. However, the basic physics of optically driven coherent THz emission are covered already by discrete three-level Bloch equations with dipole-allowed transitions between all levels as shown in Refs. [21,22]. As we have shown previously for the intracavity 2π -pulse laser generation, the substitution of a simple homogeneously broadened two-level absorber model [25] by a more realistic quantum-well absorber model using semiconductor Bloch equations [26] yields quantitative changes in the steady-state pulse duration and energy, but the very fact of intracavity self-induced transparency as well as the pulse parameter dependencies on the laser and absorber control parameter are correctly described. Moreover, for the envisaged ultrashort intracavity pulse generation with peak intensities of TW/cm^2 and a typical dipole moment of the direct interband transition ($d/e=0.3$ nm, GaAs) one obtains a peak Rabi frequency in the order of the transition frequency which is much larger than the frequency according to the excitonic binding energy ($E_{\text{ex}}=4.2$ meV, GaAs) as the characteristic strength of the Coulomb exchange interaction. Hence in the semiconductor Bloch equations [23] the enhancement of the Rabi frequency that is due to Coulomb exchange interaction can be neglected [24]. Therefore we self-consistently treat the additional THz emission during coherent quantum-well absorber mode locking in the framework of intracavity self-induced transparency in a homogeneously broadened three-level absorber. Our model describes the basic physics of an all-solid-state sub-10-fs-pulse generator with a spectral content from the THz domain to the ultraviolet in dependence on the resonator bandwidth.

The paper is organized as follows. In Sec. II we outline the resonator model with intracavity resonant three-level absorber and solid-state amplifier which are described by Maxwell-Bloch equations without RWA and SVEA. Our numerical results of SIT-pulse generation by a two-level and three-level intracavity absorber in dependence on the dipole moments, the initial population, the resonator bandwidth, and the pump rate are presented and discussed in Sec. III and the conclusions are drawn in Sec. IV.

II. BASIC EQUATIONS AND RESONATOR MODEL

We treat intracavity MSIT-pulse generation in the framework of a solid-state laser with an ultrabroadband resonator

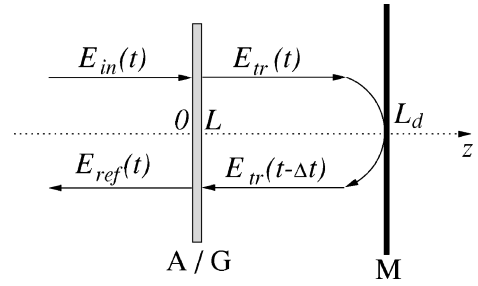


FIG. 1. Resonant layer of the absorber or gain medium with delayed feedback by an end mirror.

and an additional intracavity quantum-well absorber. At sufficient pump rates the saturable solid-state laser gain forces the multilevel absorber into the SIT regime resulting in intracavity MSIT-pulse generation. In the context of coherent absorber mode locking of solid-state lasers we have studied previously SIT-pulse formation in RWA by use of an intracavity two-level absorber [25], which aims to describe the recent generation of few-cycle optical pulses as short as 6.5 fs in duration by a Ti:sapphire laser as reported in Ref. [10]. To incorporate self-consistently THz-radiation emission from the quantum-well absorber accompanied by the ultrashort optical pulse generation as recently reported in Ref. [11] we extend our model to an intracavity three-level absorber without RWA using real fields and polarizations. An exact non-RWA description of the multilevel absorber is mandatory, because in the sub-10-fs time domain the envisaged THz-radiation emission exhibits a single to subcyclic character. In addition, also the description of few-cyclic resonant interaction of a two-level system by use of the RWA neglects important features of the population dynamics, especially inversion oscillations at twice the instantaneous frequency of the driving field, as recently studied in Refs. [27,28].

A. Resonator model

A broadband resonator is assumed to contain a solid-state amplifier, modeled by an incoherently pumped two-level system, and a coherent three-level absorber. To simplify Maxwell's equations as much as possible we consider optically thin layers of both absorber and amplifier in contact with ideal mirrors of an ultrabroadband resonator configuration (Fig. 1). Therefore during successive resonator roundtrips we consider iterative pulse shaping by coherent reflection [25] from the absorber and gain media, whereas the remaining free-space propagation and focusing by curved mirrors is effectively summarized by a frequency-dependent linear resonator transmission $T(\omega)$. The coherent reflection from a vacuum interface to a resonant medium in the region $0 < z < L$ is given by the solution of the one-dimensional boundary value problem to Maxwell's equations as [29]

$$E(z,t) = E_{\text{in}}(z,t) - \frac{2\pi}{c} \int_0^L \frac{\partial}{\partial t} P\left(z',t - \frac{|z-z'|}{c}\right) dz'. \quad (1)$$

Here $E_{\text{in}}(z,t)$ is an incident field from the left half space $z < 0$, given by a vacuum solution to the homogeneous Maxwell equations and $P(z,t)$ is the resonant macroscopic polarization of the absorber $0 < z < L$. At any space-time point

(z, t) the resultant field $E(z, t)$ is a superposition of the incident field $E_{\text{in}}(z, t)$ and the sum over the retarded induced polarization current $(\partial/\partial t)P(z', t - |z - z'|/c)$ throughout the absorber $0 < z' < L$. For an optically thin layer $L \ll \lambda$ the latter gives for the Rabi frequency of the coherently reflected wave from the absorber or gain medium

$$\Omega_{\text{coh ref}}(t) = -\alpha_{a,g} \frac{d}{dt} u_{a,g}(t), \quad (2)$$

where the Rabi frequency of the real electric field $\Omega(t) = d_a E(t)/\hbar$ is defined throughout corresponding to the dipole moment of the largest absorber transition d_a , u_a is the sum of the real parts of the multilevel absorber off-diagonal density matrix elements, and u_g is the real part of the off-diagonal density matrix element for the gain medium. The light-matter coupling constants of the thin absorber and gain, respectively, are given by $\alpha_a = 2\pi d_a^2 N_a L_a / \hbar c$ and $\alpha_g = 2\pi d_g d_a N_g L_g / \hbar c$ with length $L_{a,g} \ll \lambda$, dipole moments $d_{a,g}$, and density of resonant systems $N_{a,g}$. In what follows we characterize both the coherent absorber and gain medium by their associated superradiance times that are related to their coupling constants $\alpha_{a,g}$ and the transition frequency ω by $T_R^{a,g} = 1/\alpha_{a,g}\omega$. For pulses longer than the characteristic dephasing times $\tau_p \gg \tau_{a,g}$ the small signal absorption or gain is simply given by $\tau_{a,g}/T_R^{a,g}$. Note that the assumption of an optically thin layer works well for the 10-nm-thick quantum-well absorber used in the experiments of Refs. [10,11], but for the 1-mm-thick Ti:sapphire laser rod it results in neglect of pulse reshaping due to propagation through the amplifier. However, the principal ultrashort pulse shaping effects of the solid-state amplifier are described exactly in the scope of a non-RWA two-level system.

We consider the thin resonant layer in close contact to a resonator end mirror [10] (see Fig. 1) in a way that the coherently reflected field from the resonant layer Eq. (2) constructively interferes with the linear reflected field from the end mirror. For the structure of Fig. 1 it yields the following equations for the Rabi frequencies of the reflected (ref), transmitted (tr), and the intrinsic (intr) field inside the resonant layer, in dependence on the incident (in) field and the induced polarization current of the layer [25]:

$$\Omega_{\text{ref}}(t) = R e^{2iKL_d} \Omega_{\text{tr}}(t - \Delta t) - \alpha_{a,g} \frac{d}{dt} u_{a,g}(t), \quad (3)$$

$$\Omega_{\text{tr}}(t) = \Omega_{\text{in}}(t) - \alpha_{a,g} \frac{d}{dt} u_{a,g}(t), \quad (4)$$

$$\Omega_{\text{intr}}(t) = \Omega_{\text{tr}}(t) + \text{Re}^{2iKL_d} \Omega_{\text{tr}}(t - \Delta t). \quad (5)$$

The delayed feedback due to a metallic end mirror that is contacted at a distance $L_d \ll \lambda$ (Fig. 1) is characterized by a complex reflectivity $R = |R|e^{i\Delta\phi}$, a standing-wave phase shift $2KL_d$ with wave number K and a temporal delay of the wave $\Delta t = 2L_d/c \ll T_{\text{cyc}}$, where T_{cyc} is the period of an optical cycle. Note that the intrinsic field inside the resonant layer, which drives the coherent polarization, already contains the contribution of the induced polarization current. In what follows we assume optimal contact with $|R|=1$ and $\Delta\phi + 2KL_d = 0$, which effectively doubles the intrinsic field.

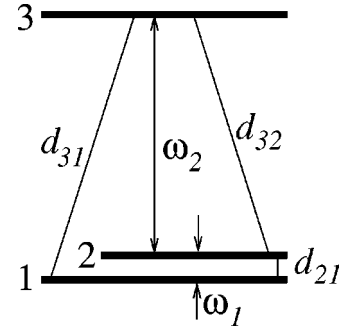


FIG. 2. Three-level system with dipole-allowed transitions between all levels. The dipole moment of the infrared transition 1-2 is thought to be externally controllable.

A resonator round-trip, consisting of subsequent reflections at the gain and absorber structure (Fig. 1), is completed by applying to the field an overall linear resonator transmission function $T(\omega)$ of bandwidth $\Delta\omega$ and a stepwise spectral dependence according to

$$T(\omega) = \begin{cases} 0, & \omega < \omega_g - \frac{\Delta\omega}{2} \\ T_0, & \omega_g - \frac{\Delta\omega}{2} < \omega < \omega_g + \frac{\Delta\omega}{2} \\ 0, & \omega > \omega_g + \frac{\Delta\omega}{2} \end{cases} \quad (6)$$

which is centered at the amplifier maximum ω_g .

B. Three-level absorber

A unified description of optical resonance phenomena in N -level systems has been achieved in the framework of a generalized $(N^2 - 1)$ -dimensional Bloch vector rotation because of the underlying $SU(N)$ symmetry [30,31]. The $SU(N)$ symmetry group reveals the existence of N constants of motion $C_n = \text{Tr}\{\hat{\rho}^n\}$, $n = 1, \dots, N$, where ρ_{ij} is the density matrix. With $\rho_{ii,0}$ being the incoherent initial population the conserved quantities can be calculated as $C_1 = \sum_i \rho_{ii}(t)$, ensuring the conservation of probability, $C_2 = \sum_i \rho_{ii,0}^2$, expressing the conservation of the Bloch vector length and for a three-level system also the higher order nonlinear constant of motion $C_3 = \sum_i \rho_{ii,0}^3$ exists. The knowledge of the constants of motion in a high-dimensional dynamic system allows an immediate insight into the dynamics without an explicit solution [31]. The eight-dimensional Bloch vector of the three-level system $\vec{S} = (u_1, u_2, u_3, v_1, v_2, v_3, w_1, w_2)$ is related to the density matrix elements by $p_1 = 2\rho_{12}$, $p_2 = 2\rho_{23}$, $p_3 = 2\rho_{13}$, $w_1 = \rho_{22} - \rho_{11}$, $w_2 = (2\rho_{33} - \rho_{22} - \rho_{11})/\sqrt{3}$ [31], $p_i = u_i + iv_i$. Without adopting the usual RWA or SVEA we obtain in relaxation time approximation the complete three-level Bloch equations for dipole-allowed transitions between all quantum levels (Fig. 2) in the following form:

$$\frac{d}{dt} p_1 + \left(\frac{1}{\tau_a} - i\omega_1 \right) p_1 = i\Omega_{\text{intr}} (2\eta_1 w_1 + p_2^* - \eta_2 p_3), \quad (7)$$

$$\frac{d}{dt}p_2 + \left(\frac{1}{\tau_a} - i\omega_2\right)p_2 = i\Omega_{\text{intr}}[\eta_2(\sqrt{3}w_2 - w_1) + \eta_1p_3 - p_1^*], \quad (8)$$

$$\begin{aligned} \frac{d}{dt}p_3 + \left[\frac{1}{\tau_a} - i(\omega_1 + \omega_2)\right]p_3 \\ = i\Omega_{\text{intr}}(\sqrt{3}w_2 + w_1 + \eta_1p_2 - \eta_2p_1), \end{aligned} \quad (9)$$

$$\frac{d}{dt}w_1 + \frac{w_1 - w_1^0}{T_a} = -\Omega_{\text{intr}}\text{Im}(2\eta_1p_1 - \eta_2p_2 + p_3), \quad (10)$$

$$\frac{d}{dt}w_2 + \frac{w_2 - w_2^0}{T_a} = -\Omega_{\text{intr}}\text{Im}(\sqrt{3}\eta_2p_2 + \sqrt{3}p_3). \quad (11)$$

The three-level Bloch equations (7)–(11) of a thin absorber with feedback mirror (see Fig. 1) are driven by the Rabi frequency of the intrinsic field inside the absorber Ω_{intr} according to Eq. (5) which self-consistently contains the induced polarization current that is responsible for the coherently reflected field, Eq. (3). The dipole moments of the intermediate absorber level (2) to the lower (1) and upper level (3) are related to the 1-3 transition dipole moment by $\eta_1 = d_{21}^a/d_{31}^a$, $\eta_2 = d_{32}^a/d_{31}^a$. The transition frequency ω_1 in Eq. (7) relates to the infrared 1-2 transition and ω_2 in Eq. (8) relates to the second optical transition 2-3 (see Fig. 2). If relaxation is negligible ($T_a, \tau_a \gg \tau_p$) the length of the three-level Bloch vector $|\vec{S}|^2 = 4[1/3 + \rho_{22,0}(\rho_{22,0} - 1) + \rho_{11,0}(\rho_{11,0} - 1) + \rho_{22,0}\rho_{11,0}]$, as a combination of the constants of motion $C_{1,2}$, will be conserved during coherent rotation according to Eqs. (7)–(11).

To solve the three-level Bloch equation system, Eqs. (7)–(11), in the transition region $\tau_p^{-1} \approx \omega_1 + \omega_2$, which is most relevant for Ti:sapphire laser pulse generation as reported in Refs. [10,11], one has to resort to numerics, as will be done below. As always, only in the limiting cases a substantial simplification of Eqs. (7)–(11) is possible. First, for long characteristic pulse durations $\tau_p^{-1} \ll \omega_2, \omega_1$, by introduction of different-wavelength pulses with slowly varying envelopes, resonant only with their corresponding transitions, and by use of the RWA one arrives at a simulton problem similar to that studied by Konopnicki and Eberly [4]. Second, in the ultratransient regime $\tau_p^{-1} \gg \omega_1 + \omega_2$, which requires attosecond pulse durations in the optical domain, it is possible to diagonalize the three-level Bloch equations with respect to the eigenmodes of the imaginary parts of the off-diagonal elements

$$\begin{aligned} v_i(t) &= -\beta_i \sin[\xi_i \Theta(t)] \quad (i=1,2,3), \\ \Theta(t) &= \int_{-\infty}^t \Omega_{\text{intr}}(t') dt'. \end{aligned} \quad (12)$$

The eigenfrequencies $\xi_i(\eta_{1,2})$ are governed by the roots of a cubic determinant:

$$\xi_1 = \sqrt{2} \sqrt{1 + \eta_1^2 + \eta_2^2 - \rho^{1/3} \cos(\phi/3)}, \quad (13)$$

$$\xi_2 = \sqrt{2} \sqrt{1 + \eta_1^2 + \eta_2^2 - \rho^{1/3} \cos[(\phi + 2\pi)/3]}, \quad (14)$$

$$\xi_3 = \sqrt{2} \sqrt{1 + \eta_1^2 + \eta_2^2 - \rho^{1/3} \cos[(\phi + 4\pi)/3]}, \quad (15)$$

with $\rho = p^{3/2}$, $\cos \phi = -q/2\rho$, and

$$p = \eta_1^4 + 3\eta_1\eta_2^2 + \eta_1^2(2 - \eta_2^2) + (1 + \eta_2^2)^2, \quad (16)$$

$$\begin{aligned} q &= 2\eta_1^6 - 3\eta_1(3\eta_2^2 - \eta_1^3)(2 - \eta_2^2) + 2(1 + \eta_2^2)^3 \\ &\quad + 3\eta_1^2(2 + 3\eta_1\eta_2^2 - 26\eta_2^2 - \eta_2^4). \end{aligned} \quad (17)$$

At particular combinations of nonzero dipole moments of all three transitions, one eigenfrequency identically vanishes, e.g., $\xi_1|_{\eta_1=\eta_2=1} = 0$, resulting in an ultratransient polarization trapping analogous to coherent population trapping in EIT. Such ultratransient polarization trapping in three-level systems relies always on the existence of specific nonzero dipole moments between all three transitions. The eigenmode amplitude ratios $\epsilon_{1,2}(\eta_{1,2}) = \beta_{1,2}/\beta_3$ are governed by the solution of the diagonalized equation system, whereas the remaining free amplitude β_3 will be fixed by the conservation law for the length of the Bloch vector. The eigenmode solution for the imaginary parts of the off-diagonal matrix elements $v_i(t) = -\beta_i \sin[\xi_i \Theta(t)]$ permits an explicit expression for the real macroscopic polarization current as driver of Maxwell's equation, Eq. (1), with the macroscopic polarization $P_a = N_a d_{31}^a u_a$, $u_a = \eta_1 u_1 + \eta_2 u_2 + u_3$, and

$$\begin{aligned} \frac{d}{dt}u_a(t) &= -\beta_3(\omega_1 + \omega_2) \left(\frac{\omega_1}{\omega_1 + \omega_2} \eta_1 \epsilon_1 \sin[\xi_1 \Theta(t)] \right. \\ &\quad \left. + \frac{\omega_2}{\omega_1 + \omega_2} \eta_2 \epsilon_2 \sin[\xi_2 \Theta(t)] + \sin[\xi_3 \Theta(t)] \right). \end{aligned} \quad (18)$$

C. Solid-state amplifier

We consider a coherent intracavity absorber that is placed inside an ultrabroadband resonator together with a solid-state laser gain medium described by two-level Bloch equations

$$\frac{d}{dt}p_g + \left(\frac{1}{\tau_g} - i\omega_g\right)p_g = 2i\eta_g\Omega_{\text{intr}}w_g, \quad (19)$$

$$\frac{d}{dt}w_g + \frac{w_g - w_g^0}{T_g} = -2\eta_g\Omega_{\text{intr}}\text{Im}(p_g), \quad (20)$$

where $w_g^0 > 0$ accounts for stationary incoherent pumping and $\eta_g = d_{21}^g \sqrt{A_a/d_{31}^g} \sqrt{A_g}$ is the effective ratio of the dipole moments of the gain and the 1-3 absorber transition including the effective beam cross section in the absorber and gain, respectively. As for the absorber, the amplifier Bloch equations are driven by the intrinsic field inside the amplifier Ω_{intr} according to Eq. (5). The real macroscopic polarization of the gain medium is given by $P_g = N_g d_{21}^g u_g$, with the real part of the complex off-diagonal matrix element $p_g = u_g + i v_g$.

The solid-state amplifier works in the incoherent linear regime with $\eta_g \Omega_{\text{intr}}^{\text{max}} \ll 1$ corresponding to the Ti:sapphire laser with an intracavity coherent GaAs quantum-well absorber of Refs. [10,11]. Since the envisaged generation of ultrashort optical pulses involves a huge number of resonator modes, i.e., the pulse duration in the order of the optical

cycle T_{cyc} is much shorter than the resonator round-trip time of $T_{\text{rep}} \approx 10$ ns [10], we replace the periodic boundary conditions for the field and quantum states by initial conditions in infinity and calculate the energy of the pulse by $\int_{-\infty}^{\infty} E^2(t) dt$.

To date, the Ti:sapphire laser exhibits the largest amplification bandwidth with an associated dephasing time of only $\tau_g = 2.5$ fs. Its population relaxation time $T_g \approx 3$ μ s is much larger than the resonator round-trip time T_{rep} which defines the repetition period of the emerging pulse train. Therefore from Eq. (20) we obtain that the initial inversion in the next round-trip is determined by the final inversion of the preceding round-trip according to the map [32]

$$w_{k+1}^< = w_g^0 + (w_k^> - w_g^0) \exp\left(-\frac{T_{\text{rep}}}{T_g}\right), \quad (21)$$

where $w_{k+1}^<$ is initial inversion before the pulse arrived in round-trip $k+1$ and $w_k^>$ is the final inversion after the pulse has gone in round-trip k . Since the amplifier works in the incoherent regime $\eta_g \Omega_{\text{intr}}^{\text{max}} \ll 1$, dynamic pulse reshaping that is due to the gain medium is negligible. Since $T_{\text{rep}} \ll T_g$, saturation of the amplifier is achieved by the total pulse train according to the inversion map Eq. (21).

III. NUMERICAL RESULTS OF STEADY-STATE MSIT-PULSE GENERATION

We have numerically implemented the above described resonator model and solved for solitary wave solutions by iterating an arbitrary seed pulse until a self-reproducing steady-state pulse has been reached. The parameters of the amplifier are chosen throughout to model a Ti:sapphire laser according to Refs. [10,11] with $\tau_g = 2.5$ fs, $T_g = 3$ μ s, $\omega_g = 2\pi/T_{\text{cyc}}$, $T_{\text{cyc}} = 2.8$ fs, $T_R^a = 0.1$ fs, and $\eta_g = 0.1$. The external pump is adjusted by varying the steady-state amplifier inversion $w_g^0 \approx 6-8\%$ in order to obtain intracavity pulse energies in the range $\approx 150-500$ nJ. The largest absorber transition frequency 1-3 (Fig. 2) is chosen to be equal to the amplifier transition $\omega_1 + \omega_2 = \omega_g$ and the infrared absorber transition frequency 1-2 to be $\omega_1 = (\omega_1 + \omega_2)/10$. The dipole moment of the largest absorber transition 1-3 is chosen according to the direct interband dipole moment of a GaAs absorber $d_{31}^a/e = 0.3$ nm. As absorber relaxation times we use throughout a phase relaxation time of all transitions $\tau_a = 50$ fs [33] and a population relaxation time of all levels $T_a = 100$ fs [34]. The absorber superradiance time T_R^a , which controls the strength of the light-matter interaction, will be varied between 50 and 100 fs [25]. The resonator is chosen to possess a constant round-trip time of $T_{\text{rep}} = 10$ ns and a linear transmission of $T_0 = 0.97$ with different bandwidth $\Delta\omega$.

A. SIT-pulse generation by two-level intracavity absorber

Let us start with intracavity SIT-pulse generation by a two-level absorber, setting $\eta_1 = \eta_2 = 0$ and a resonator bandwidth $\Delta\omega$ to cover the complete spectrum of the emerging SIT pulse inside the passband. In Fig. 3 the steady-state pulse, inversion, and spectrum for increasing intracavity pulse energy, i.e., pump rate, is depicted. In general, the non-RWA results extend the previous RWA-SVEA model

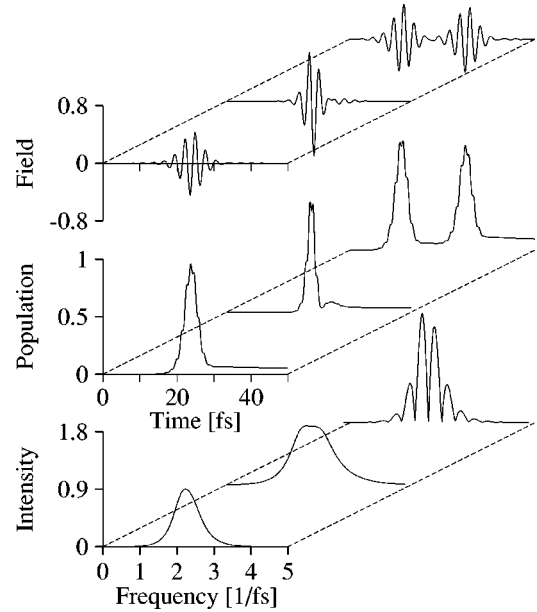


FIG. 3. Two-level absorber SIT-pulse generation. Electric field, ground-state population, and spectral intensity of the steady-state pulse due to an intracavity two-level absorber with $T_R^a = 50$ fs. The pulse energy is 154 nJ (front), 280 nJ (middle), 328 nJ (background). Throughout, the electric field is normalized by $E_0 = 2 \times 10^7$ V/cm corresponding to a Rabi frequency $\Omega_0 = 1$ fs $^{-1}$ and intensity $I_0 = 1.2$ TW/cm 2 .

[25] down to the single and even subcyclic domain. Below a certain threshold pulse energy, i.e., pump rate, the laser remains in the free running regime because the Rabi frequency is too weak to induce complete Rabi flopping. Above the mode locking threshold, in the SIT regime, the complete Rabi flopping of the inversion forms a stable ultrashort intracavity SIT pulse with self-reproduction during each cavity round-trip.

In difference to the RWA model which yields smooth adiabatic inversion in the self-induced transparency regime, the non-RWA calculations reveal additional modulations of the inversion (Fig. 3). These non-RWA inversion modulations result from the proportionality of the population to the instantaneous pulse energy around the extrema of the oscillating electric field [28]. This induces modulations with doubled frequency as compared to the oscillatory driving field. Hence, at each extremum of the electric field a maximum of the non-RWA population modulation occurs [28]. Between these modulation maxima the electric field crosses zero and its time derivative becomes maximum which is reflected as a minimum in the non-RWA population modulation [27,28]. As will be shown below, the amplitudes of these non-RWA modulations become greatly enhanced in the case of the three-level MSIT pulse.

For increasing energy (front to background plots, Fig. 3) we obtain pulse shortening down to a near single cyclic regime (middle plot), further increasing of the energy yields coherent pulse splitting with two complete Rabi flops of the populations (background). The flat top, dipped spectrum of the near single-cyclic pulse (middle plot) indicates transition to pulse splitting. Introduction of a pulse envelope for several-cyclic pulses recovers the 2π (front) and $2 \times 2\pi = 4\pi$ (background) envelope-area conservation of two-level

SIT [3,25]. In two-level absorber SIT the populations of the lower and upper level monotonically follow the pulse envelope with superimposed non-RWA modulations at twice the oscillation frequency of the driving electric field (see Fig. 3). In general, the monotonic following of the population with the pulse envelope will change in multilevel SIT because of the constants of motion [31].

B. MSIT-pulse generation by three-level intracavity absorber

Nowadays, intracavity quantum-well GaAs absorber are successfully used for ultrashort pulse generation [10] as well as intracavity coherent THz emitter [11]. We consider a corresponding intracavity three-level system with equal dipole moments for the direct hh and lh transitions to the conduction band $d_{31}=d_{32}$ and an inter-valence-band dipole moment d_{21} that owing to valence-band mixing is controllable externally by applying a dc bias [21]. By finding such an intracavity steady-state MSIT-pulse solution that is due to a three-level absorber we describe the generation of the optical, infrared, and, as will be shown, ultraviolet constituents of an ultrabroadband electromagnetic field pulse which drives all three levels through complete Rabi flopping. Such intracavity MSIT-pulse generation can be viewed as an all-solid-state ultrabroadband pulse generator ranging from the THz up to ultraviolet domain.

The complex non-RWA dynamics of resonant three-level systems was to our knowledge previously studied only for intense stationary bichromatic fields [35]. We study an extremely nonstationary and strong electromagnetic field which induces self-induced transparency by an ultrafast adiabatic following of all level populations with the driving field. Adiabatic following in a three-level system has been studied previously in the RWA and SVEA in Ref. [36]. It was theoretically found [36,37] and experimentally verified [38] that for adiabatic inversion of a three-level system with double-photon resonant pulses a counterintuitive excitation order is most efficient. Counterintuitive excitation means that from the two temporally overlapping pulses, the pulse which is resonant with the energetically upper transition of the three-level system has to precede the pulse which is resonant with the energetically lower transition. Hence, to adiabatically invert a three-level system it is most efficient that a first pulse strongly drives the thermally empty upper states, before a second pulse strongly interacts with the thermally populated lower states.

1. Influence of different dipole moments

We start the discussion of three-level MSIT-pulse generation from the λ configuration $\eta_1=0, \eta_2=1$ and gradually increase the dipole moment of the infrared THz transition η_1 [see Figs. 4(a)–4(d)]. Obviously, the MSIT pulse drives all level populations through increasing complex dynamics as the infrared dipole moment $0 \leq \eta_1 \leq 3$ of the 1-2 transition is increased [see curves 1,2,3 in Figs. 4(a)–4(d)]. In comparison to the two-level absorber (Fig. 3) the amplitude of the population modulation at doubled frequency of the real electric field becomes strongly enhanced. Since the population of each level is forced to Rabi flopping and simultaneously fulfills the conservation laws, the individual population of the upper level 3 (curve 3) performs two complete Rabi flops,

with a maximum population of only 0.5, whereas level 1 (curve 1) and level 2 (curve 2) perform one complete Rabi flop with almost full inversion of the infrared transition 1-2 [Fig. 4(a)]. Since we start in every round-trip from the absorber ground state (1,0,0), it is in accordance with all three conservation laws to expect a MSIT scenario of total inversion by bringing the entire population to the upper level 3. However, instead of total inversion, at its peak the MSIT pulse fully inverts only the infrared transition 1-2, whereas at the leading and trailing edges of the pulse both optical transitions become partially inverted. The fact that simultaneously with the 1-3 transition also the second optical 2-3 transition becomes partially inverted at the leading edge of the pulse, before the infrared 1-2 transition becomes inverted at the pulse peak, reveals that, besides the direct 1-3 excitation, the above mentioned counterintuitive 1-2-3 excitation is the most efficient way to excite the three-level system.

Despite the complex population dynamics, the temporal structure of the steady-state electric field consists in all situations of only four to five optical cycles with increasing asymmetry and nonmonochromaticity [Fig. 4(a)–4(d)]. The high-frequency optical components are concentrated on the leading edge of the pulse [see Fig. 4(d)], whereas the infrared components follow at the trailing edge. That again results from a counterintuitive double-photon 1-2-3 excitation yielding maximum adiabatic inversion of the three-level system [37]. It is interesting to note that our numerical round-trip model self-consistently produces a stable multicomponent pulse which naturally exhibits counterintuitive temporal ordering of the spectral components, since the stability of a pulsed laser regime requires always an improved energy extraction of the steady-state pulse in comparison to the coexisting free running laser regime. The durations of the MSIT pulses defined as full width at half maximum (FWHM) of the intensity envelope run from 7 to 10 fs. Enhancement of the infrared dipole moment up to $\eta_1=3$ yields strong increasing of the amplitude of the population modulations on the infrared transition (level 1 and 2), with full modulation depth making them indistinguishable from multiple Rabi flopping on the infrared transition. In contrast to the strongly driven infrared transition, the upper level 3 of the two optical transitions still performs two Rabi floppings with only moderate non-RWA population modulations at doubled frequency of the electric field [Figs. 4(a)–4(d)].

Besides the temporal characterization of the MSIT pulse and its self-induced population dynamics, most valuable for characterization of the steady-state MSIT pulse is its ultrabroadband spectrum as shown in Fig. 5. Obviously we find a multicomponent spectral structure. As can be seen from Fig. 5, with increasing infrared dipole moment we obtain a strong enhancement of the infrared spectral component at the transition frequency ω_1 , as well as the spectral component at the lower optical transition ω_2 . However, most significant is the strong enhancement of the optical second harmonic signal. It is necessary to emphasize that such increasing effective generation of the second and higher optical harmonics is entirely due to the non-RWA high-frequency population oscillations, which are in our coherent three-level system easily controllable by the infrared transition dipole moment $\eta_1 > 1$. Such higher harmonics production in the three-level system resembles, at least for the infrared transition, the high-

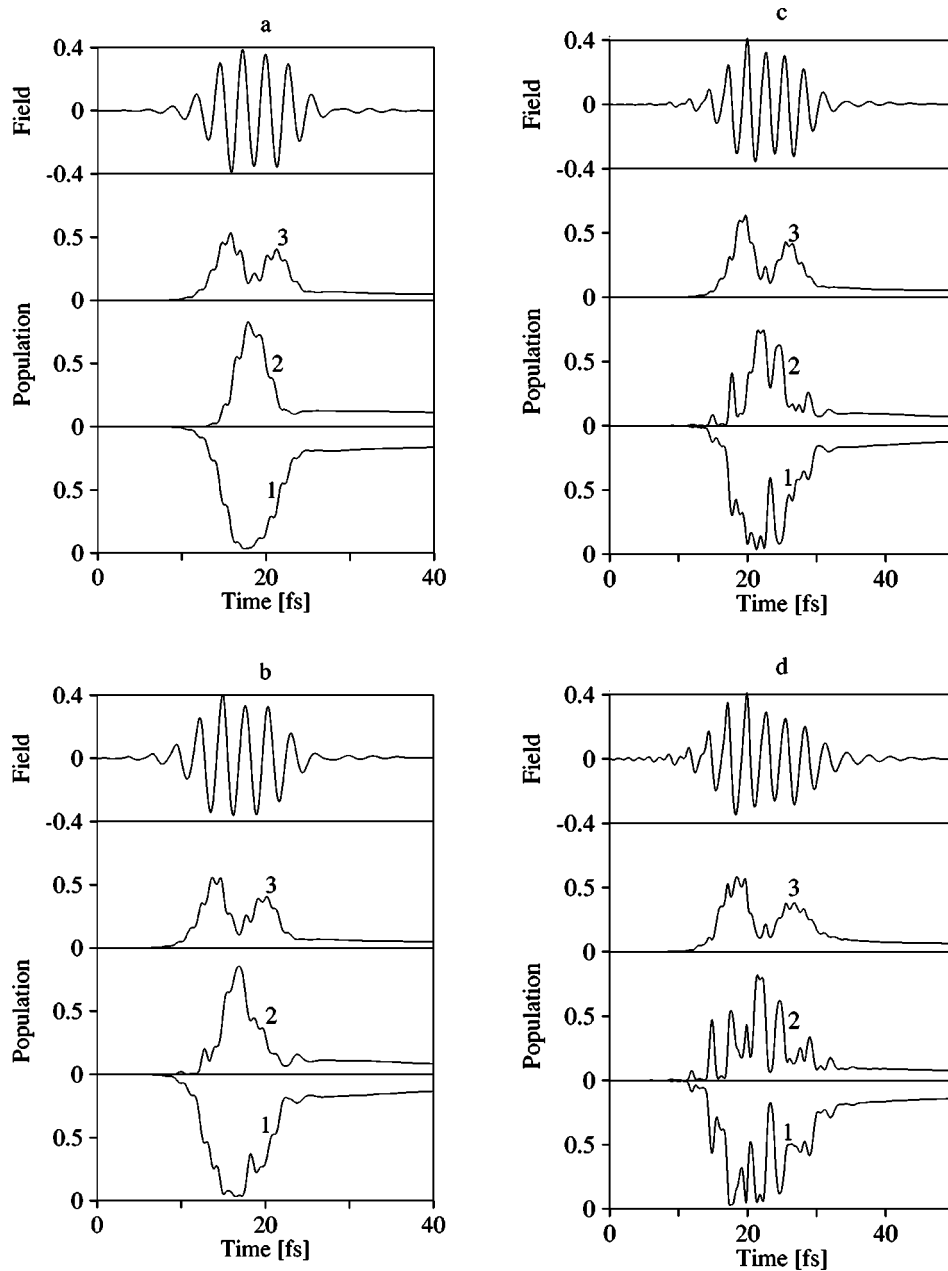


FIG. 4. Three-level absorber MSIT-pulse generation. Electric field (uppermost part) and individual level populations (lower parts) of the steady-state pulse due to an intracavity three-level absorber with $T_R^a = 100$ fs, $\eta_2 = 1$ and different infrared-transition dipole moments (a) $\eta_1 = 0$, (b) $\eta_1 = 1$, (c) $\eta_1 = 2$, (d) $\eta_1 = 3$. The pulse energy amounts always to ≈ 200 nJ. The level populations are 3 upper level, 2 intermediate level, 1 ground state. No additional bandwidth limitation due to linear resonator transmission.

harmonics generation from a superdriven two-level system as studied in Ref. [39]. Note that the second optical harmonics at the largest infrared dipole moment of $\eta_1 = 3$ reaches a peak intensity of 1/5 of the intensity of the fundamental signal [Fig. 5(d)]. For the λ configuration $\eta_1 = 0, \eta_2 = 1$ in Fig. 5(a) (long-dashed line) we depicted additionally the spectrum of the corresponding two-level SIT pulse ($\eta_1 = \eta_2 = 0$). Obviously, the characteristic side lobes of the λ system MSIT-pulse spectrum disappears for the two-level system.

Since the resonator bandwidth $\Delta\omega$ is chosen to cover the complete emerging generation spectrum, any peak from the infrared region up to the third optical harmonics is strongly individually broadened. For instance, the individual spectral width of the dominant infrared peak at ω_1 corresponds to a

single to subcyclic temporal structure. Moreover, by the coherent light-matter interaction, those spectral components which exceed the Lorentzian gain profile [dotted line, Figs. 5(b)–5(d)] experiences gain by a temporarily stimulated emission process. Note that our simple coherent three-level absorber yields principal emission peaks at exactly the maxima of the absorption spectrum, corresponding to the transition frequencies $\omega_1, \omega_2, \omega_1 + \omega_2$. The increasing spectral complexity in Fig. 5 is due to the non-RWA coherent three-level dynamics. In contrast, a more sophisticated quantum-well absorber model, which is based on three-band semiconductor Bloch equations (SBE) [19] with inhomogeneous broadening due to freely movable carriers and its Coulomb interaction yields a shift and splitting of the THz-

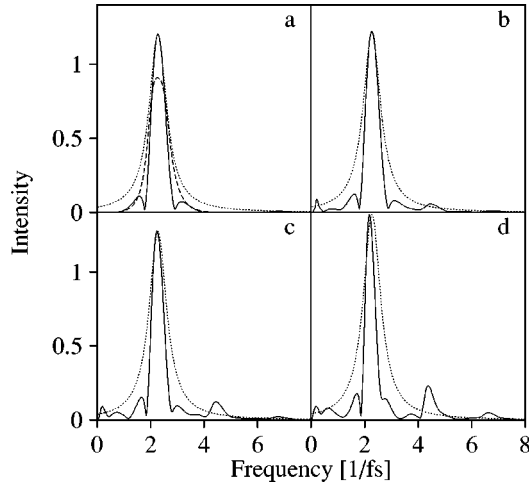


FIG. 5. Spectrum of three-level MSIT pulses. Spectral intensity versus angular frequency for different infrared-transition dipole moments according to Fig. 4. The dotted lines depict the Lorentzian gain profile with bandwidth corresponding to $\tau_g = 2.5$ fs centered at $\omega_g = \omega_{31}$, the long-dashed line in the case (a) depicts the spectral intensity of a two-level SIT pulse with $T_R^a = 100$ fs and a pulse energy of 180 nJ just below coherent pulse splitting. No additional bandwidth limitation due to linear resonator transmission.

emission peak in comparison to the absorption line. Note that the validity of a SBE description of THz emission from a quantum-well absorber is somewhat controversial [40]. Our focus in dealing with a simple coherent three-level absorber model is to study exactly the non-RWA interaction dynamics of ultrabroadband electromagnetic pulses, especially to prove the existence of intracavity MSIT pulses in a solid-state laser resonator. Regarding the underlying coherent three-level dynamics, the most important quantum-well specific feature is an externally controllable dipole moment of the infrared transition 1-2, yielding a three-level system with dipole-allowed transitions between all levels. This point substantially differs from conventional atomic three-level systems, where the symmetry of the wave functions requires at least one of the three dipole moments to vanish.

2. Influence of pulse energy

As for the SIT-pulse generation by a two-level absorber, the MSIT-pulse generation by a multilevel absorber requires a minimum pulse energy, i.e., pump rate, below which the laser remains in free running operation. Increasing of the pulse energy yields shortening of the pulse. Analogous to the SIT-pulse generation by a two-level absorber (Fig. 3), the MSIT-pulse generation by the three-level absorber exhibits coherent pulse splitting too, at an increased pulse energy which is sufficient to provoke two times excitation and returning of the population to the initial state. In Fig. 6 we have plotted the electric field and the population of all levels (curves 1,2,3) for MSIT-pulse splitting in a three-level system with $\eta_1 = \eta_2 = 1$ and a total pulse energy of 544 nJ, i.e., approximately 272 nJ for each individual pulse. Unlike SIT-pulse generation by the two-level absorber, where pulse splitting always occurs at increased energies, for three-level MSIT-pulse formation at large infrared dipole moments η_1

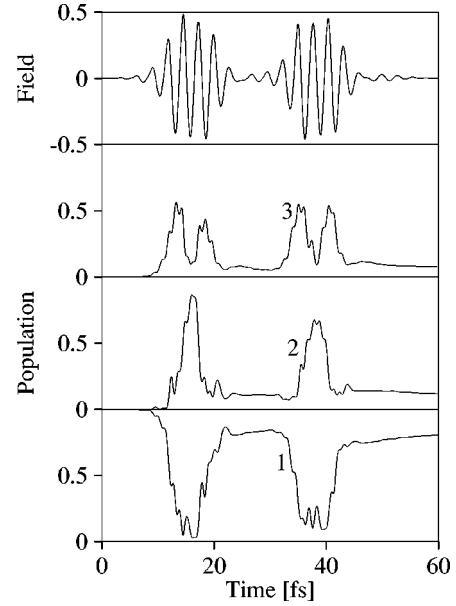


FIG. 6. Coherent three-level MSIT-pulse splitting. Electric field (uppermost part), and individual level populations (lower parts) of the steady-state pulse due to an intracavity three-level absorber with $T_R^a = 100$ fs, $\eta_1 = \eta_2 = 1$ at a pulse energy of 544 nJ. The level populations are 3 upper level, 2 intermediate level, 1 ground state. No additional bandwidth limitation due to linear resonator transmission.

$> \eta_2$ we did not observe steady-state pulse splitting at enlarged energies since for elevated pump rates there exists no steady-state pulse at all.

3. Influence of different initial populations

Throughout the preceding discussion of three-level MSIT-pulse generation we started from incoherent initial populations of level 1,2,3 as (1,0,0), respectively, which corresponds to an equilibrium initial distribution at low temperatures ($k_B T \ll \hbar \omega_1$) on the infrared transition. At a finite-temperature initial population distribution as $(\frac{2}{3}, \frac{1}{3}, 0)$ the resulting steady-state MSIT pulse is depicted in Fig. 7. Here the magnitude of Rabi flopping is decreased because of the constraints by the three conserved quantities $C_1 = 1, C_2 = 5/9, C_3 = 1/3$ which restrict the amplitude of the population dynamics on the intermediate level 2 (curve 2), whereas the population of the upper level 3 (curve 3, Fig. 7) performs again twice Rabi flopping as in Figs. 4(a)–4(d) for (1,0,0). Both the infrared spectral component and the higher order harmonics becomes increasingly suppressed for $(\frac{2}{3}, \frac{1}{3}, 0)$ [Fig. 8(a)] until they vanish completely for an equilibrium initial distribution at high temperatures ($k_B T \gg \hbar \omega_1$) on the infrared transition $(\frac{1}{2}, \frac{1}{2}, 0)$ [Fig. 8(b)].

4. Influence of resonator bandwidth

Up to now we have studied MSIT-pulse generation by a three-level absorber inside an idealized solid-state laser resonator with sufficient bandwidth to cover the complete emerging MSIT-pulse spectrum inside the passband. To figure out the influence of finite feedback bandwidth on the MSIT-pulse generation, we repeated the calculations of Fig. 4(d)

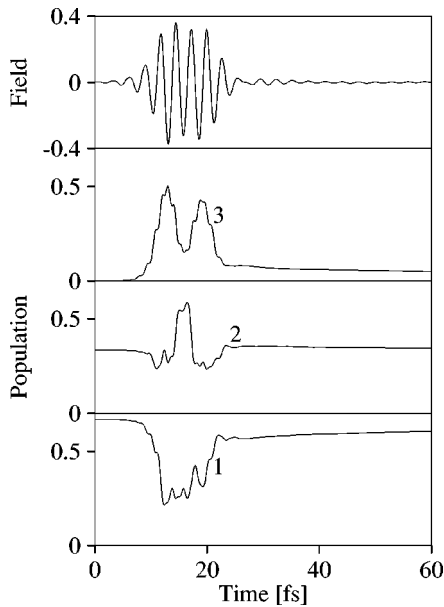


FIG. 7. Influence of different initial populations on three-level MSIT-pulse generation. Electric field, and individual level populations of the steady-state pulse due to an intracavity three-level absorber with $T_R^a = 100$ fs, $\eta_1 = \eta_2 = 1$ at a pulse energy of 200 nJ. The initial populations are $\rho_{11,0} = 2/3$ and $\rho_{22,0} = 1/3$. The level populations are 3 upper level, 2 intermediate level, 1 ground state. No additional bandwidth limitation due to linear resonator transmission.

with a typical Ti:sapphire laser bandwidth of $\Delta\lambda = 400$ nm centered at 800 nm [10]. For an infrared dipole moment of $\eta_1 = 3$ we redraw in Fig. 9 simultaneously the spectral intensities of the MSIT pulses due to a $\Delta\lambda = 400$ nm resonator (solid line) and an infinite bandwidth resonator (long-dashed line). Obviously, all spectral components outside the resonator's passband (arrows) are diminished, but in a nonmonotonous way, suppressing the infrared component to much less of an extent than the predominantly suppressed higher optical harmonics. Thus, in the case of usual resonator bandwidth $\Delta\lambda = 400$ nm, the lack of feedback for the ultraviolet region of the MSIT suppresses strongly the non-RWA high-harmonic population oscillations on the infrared 1-2 transition, which would be present for the ultrabroad-bandwidth resonator [see Fig. 4(d)]. As can be seen from Fig. 9, the efficiency of frequency conversion that is due to an additionally introduced THz emitter inside a conventional narrow

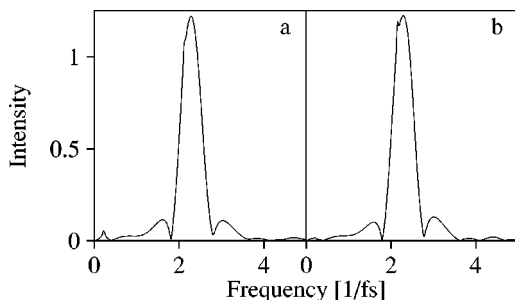


FIG. 8. Spectral intensity versus angular frequency for different initial populations (a) $\rho_{11,0} = 2/3$, $\rho_{22,0} = 1/3$ and (b) $\rho_{11,0} = \rho_{22,0} = 1/2$ and other parameters according to Fig. 7. No additional bandwidth limitation due to linear resonator transmission.

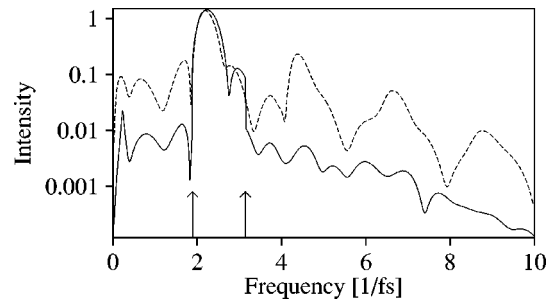


FIG. 9. Influence of resonator bandwidth. Solid line: spectral intensity versus angular frequency for $T_R^a = 100$ fs, $\eta_1 = 3$, $\eta_2 = 1$ at a pulse energy of 219 nJ and a finite resonator bandwidth of $\Delta\lambda = 400$ nm centered at 800 nm. Dotted line: the same for infinite resonator bandwidth [as in Fig. 5(d)] with energy 217 nJ. The arrows indicate the spectral limits of the resonator passband.

bandwidth solid-state laser resonator is much less than that owing to non-RWA frequency generation that is due to MSIT-pulse generation by an intracavity three-level absorber inside a resonator with enhanced feedback bandwidth.

IV. CONCLUSION

Recent experiments dealing with the intracavity usage of GaAs single quantum-well absorbers to generate ultrashort optical pulses [10] as well as coherently induced THz-radiation emission from a mode-locked solid-state laser [11] are self-consistently addressed by exact multilevel Maxwell-Bloch equations without RWA and SVEA at a unified basis of multilevel self-induced transparency in a three-level absorber combined with an effective two-level solid-state amplifier inside an ultrabroadband resonator. Unlike the experiment in Ref. [11], the mode locking and the infrared emission is achieved by one coherent three-level absorber only. We have shown that a broadband resonator with solid-state laser gain medium and an intracavity three-level absorber permits the generation of ultrabroadband electric field pulses by non-RWA frequency mixing during multilevel self-induced transparency. The dependence of intracavity MSIT on the absorber dipole moments, initial population, as well as on the laser pump rate and the resonator bandwidth has been discussed. For sufficient resonator bandwidth and infrared dipole moment we have found the spectrum of the three-level MSIT pulse to be extended from the infrared region up to the third optical harmonic at an averaged side lobe suppression ratio as low as only one order of magnitude compared to the principal optical laser spectrum. For chosen parameters of the GaAs single quantum-well absorber and Ti:sapphire laser in correspondence to the experiments in Refs. [10,11] our model predicts steady-state MSIT pulses with energies and durations which are in close agreement with experimental data [10,11]. At increased absorber density and elevated pulse energy, i.e., laser pump rate, we find near single-cyclic MSIT-pulse generation as well as coherent MSIT-pulse splitting.

ACKNOWLEDGMENT

V.P. Kalosha gratefully acknowledges support from the Alexander von Humboldt Foundation.

- [1] S. E. Harris, Phys. Rev. Lett. **70**, 552 (1992); **72**, 52 (1994).
- [2] J. H. Eberly, M. L. Pons, and H. R. Haq, Phys. Rev. Lett. **72**, 56 (1994).
- [3] S. L. McCall and E. Hahn, Phys. Rev. Lett. **18**, 908 (1967).
- [4] M. J. Konopnicki and J. H. Eberly, Phys. Rev. A **24**, 2567 (1981).
- [5] É. M. Belenov and I. A. Poluékto, Sov. Phys. JETP **29**, 754 (1969).
- [6] N. Tan-No and K. Yokoto, Phys. Rev. Lett. **29**, 1211 (1972).
- [7] F. T. Hioe and R. Grobe, Phys. Rev. Lett. **73**, 2559 (1994).
- [8] G. Vemuri, G. S. Agarwal, and K. V. Vasavada, Phys. Rev. Lett. **79**, 3889 (1997).
- [9] V. S. Butylkin, A. E. Kaplan, Y. G. Khronopulo, and E. I. Yakubovich, *Resonant Nonlinear Interactions of Light with Matter* (Springer-Verlag, Berlin, 1989).
- [10] I. D. Jung, F. X. Kärtner, N. Matuschek, D. H. Sutter, F. Morier-Genoud, G. Zhang, U. Keller, V. Scheuer, M. Tilsch, and T. Tschudi, Opt. Lett. **22**, 1009 (1997).
- [11] N. Sarukura, Z. Liu, H. Ohtake, S. Izumida, T. Yamanaka, Y. Segawa, T. Itatani, T. Sugaya, T. Nakagawa, and Y. Sugiyama, Jpn. J. Appl. Phys., Part 2 **36**, L560 (1997).
- [12] A. Bonvalet, M. Joffre, J. L. Martin, and A. Migus, Appl. Phys. Lett. **67**, 2907 (1995).
- [13] M. Joschko, M. Woerner, Th. Elsaesser, E. Binder, T. Kuhn, R. Hey, H. Kostial, and K. Ploog, Phys. Rev. Lett. **78**, 737 (1997).
- [14] P. C. M. Plancken, M. C. Nuss, I. Brener, K. W. Gossen, M. S. C. Luo, L. Chuang, and L. N. Pfeiffer, Phys. Rev. Lett. **69**, 3800 (1992).
- [15] H. G. Roskos, M. C. Nuss, J. Shah, D. A. B. Miller, S. Schmitt-Rink, and K. Köhler, Phys. Rev. Lett. **68**, 2216 (1992).
- [16] A. Bonvalet, J. Nagle, V. Berger, A. Migus, J. L. Martin, and M. Joffre, Phys. Rev. Lett. **76**, 4392 (1996).
- [17] C. Waschke, H. G. Roskos, R. Schwedler, K. Leo, H. Kurz, and K. Köhler, Phys. Rev. Lett. **70**, 3319 (1993).
- [18] L. Tsang, Ch. Chansungsan, and S. L. Chuang, Phys. Rev. B **45**, 11 918 (1992).
- [19] E. Binder, T. Kuhn, and G. Mahler, Phys. Rev. B **50**, 18 319 (1994).
- [20] Ch. Chansungsan, L. Tsang, and S. L. Chuang, J. Opt. Soc. Am. B **11**, 2508 (1994); Ch. Chansungsan, *ibid.* **13**, 2792 (1996).
- [21] M. S. C. Luo, S. L. Chuang, P. C. M. Plancken, I. Brener, H. G. Roskos, and M. C. Nuss, IEEE J. Quantum Electron **30**, 1478 (1994).
- [22] M. C. Nuss, P. C. M. Plancken, I. Brener, H. G. Roskos, M. S. C. Luo, and S. L. Chuang, Appl. Phys. B: Lasers Opt. **58**, 249 (1994).
- [23] H. Haug and S. W. Koch, *Quantum Theory of the Optical and Electronic Properties of Semiconductors*, 2nd ed. (World Scientific, Singapore, 1993).
- [24] Th. Östreich and A. Knorr, Phys. Rev. B **48**, 17 811 (1993).
- [25] V. P. Kalosha, M. Müller, and J. Herrmann, Opt. Lett. **23**, 117 (1998).
- [26] M. Müller, V. P. Kalosha, and J. Herrmann, Opt. Commun. (to be published).
- [27] R. W. Ziolkowski, J. M. Arnold, and D. M. Gogny, Phys. Rev. A **52**, 3082 (1995).
- [28] L. W. Casperson, Phys. Rev. A **57**, 609 (1998).
- [29] M. G. Benedict and E. D. Trifonov, Phys. Rev. A **38**, 2854 (1988).
- [30] J. N. Elgin, Phys. Lett. **80A**, 140 (1980).
- [31] F. T. Hioe and J. H. Eberly, Phys. Rev. Lett. **47**, 838 (1981).
- [32] V. P. Kalosha, M. Müller, J. Herrmann, and S. Gatz, J. Opt. Soc. Am. B **15**, 535 (1998).
- [33] J. Y. Bigot, M. T. Portella, R. W. Schoenlein, J. E. Cunningham, and C. V. Shank, Phys. Rev. Lett. **67**, 636 (1991).
- [34] Th. Elsässer, J. Shah, L. Rota, and P. Lugli, Phys. Rev. Lett. **66**, 1757 (1991).
- [35] T. S. Ho and S. I. Chu, Phys. Rev. A **31**, 659 (1985).
- [36] J. Oreg, F. T. Hioe, and J. H. Eberly, Phys. Rev. A **29**, 690 (1984).
- [37] C. E. Carroll and F. T. Hioe, Phys. Rev. A **42**, 1522 (1990).
- [38] U. Gaubatz, P. Rudecki, M. Becker, S. Schieman, M. Külz, and K. Bergmann, Chem. Phys. Lett. **149**, 463 (1988).
- [39] A. E. Kaplan and P. L. Shkolnikov, Phys. Rev. A **49**, 1275 (1994).
- [40] V. M. Axt, G. Bartels, and A. Stahl, Phys. Rev. Lett. **76**, 2543 (1996).